



## Controlling the oxide film destruction, metal dissolution, and H<sub>2</sub> generation on Al in acid solutions

M. Alfakeer<sup>a,\*</sup>, S. Abd El Wanees<sup>b,c,\*</sup>, H. Hawsawi<sup>d</sup>, Salih S. Al-Juaid<sup>e</sup>,  
Ameena M. Al-bonayan<sup>f</sup>, M. Abdallah<sup>f,g</sup>, Salah S. Elyan<sup>h</sup>

<sup>a</sup>Chemistry Department, Faculty of Science, Princess Nourah bint Abdulrahman University, Riyadh, Saudi Arabia, email: msalonazi@pnu.edu.sa

<sup>b</sup>University College of Umluj, Umluj, University of Tabuk, Tabuk, Saudi Arabia, email: s\_nasr@ut.edu.sa

<sup>c</sup>Chemistry Department, Faculty of Science, Zagazig University, Zagazig 44519, Egypt, email: s\_wanees@yahoo.com

<sup>d</sup>University College of Alwajh, Alwajh, Tabuk University, Tabuk, Saudi Arabia, email: hnoho60@gmail.com

<sup>e</sup>Chemistry Department Faculty of Science, King Abdulaziz University, Jeddah, Saudi Arabia, email: Salih\_aljuaid@hotmail.com

<sup>f</sup>Chemistry Department, Faculty of Applied Science, Umm Al-Qura University, Makkah, Saudi Arabia, email: benayana@hotmail.com

<sup>g</sup>Chemistry Department, Faculty of Science, Benha University, Benha, Egypt, email: metwally555@yahoo.com/maabdelsaid@uqu.edu.sa

<sup>h</sup>School of Biotechnology, Badr University in Cairo, Badr City, Cairo 11829, email: salah.abosalem1@gmail.com

Received 14 August 2022; Accepted 18 January 2023

### ABSTRACT

Two kinds of dihydropyridine derivatives, namely, 2-oxo-1,2-dihydropyridine-3-carboxylic acid (ODCA) and 2-oxo-6-phenyl-1,2-dihydropyridine-3-carboxylic acid (OPDCA) were utilized as controllers for the destruction of Al<sub>2</sub>O<sub>3</sub> film, corrosion of Al and H<sub>2</sub> production on Al surface in 2.0 M HCl solutions. Chemical (weight loss, open-circuit potential, gasometry) and electrochemical techniques (galvanostatic polarization, and electrochemical impedance spectroscopy) with the surface investigation of some corroded Al samples by a scanning electron microscope were used. The rate of H<sub>2</sub> production increased with the immersion time (*t*) and temperature (*T*) and was mitigated in the presence of ODCA and OPDCA inhibitors. Galvanostatic polarization data indicated that the used compounds behaved as mixed-type inhibitors by the formation of an adsorbed film on the Al surface. The thermodynamic parameters,  $\Delta G_{\text{ads}}^{\circ}$  and  $K_{\text{ads}}$  assured spontaneous mixed physical and chemisorption mechanisms.

**Keywords:** Oxide film destruction; Hydrogen production; Corrosion inhibition; Aluminium; Dihydropyridine derivatives

### 1. Introduction

The study of the electrochemical behavior of Al and Al alloys is considered an important subject of research due to their roomy use in daily life. The resistance of Al to the corrosion process in an aqueous neutral borate solution is based on the presence of Al<sub>2</sub>O<sub>3</sub> film that is linked hardly to the metal surface. Generally, the formed Al<sub>2</sub>O<sub>3</sub> film is composed of two layers [1], the inner Al<sub>2</sub>O<sub>3</sub> film adjacent to the

metal is compact, and its thickness is constant during ionization and decreased with temperature, the outer Al<sub>2</sub>O<sub>3</sub> film is porous and continues to grow [1]. On the other hand, Uhlig and Revie [2] demonstrated that the passive film formed on the metal surface is a chemisorbed layer of O<sub>2</sub>. The thickness of the air-formed oxide film on the Al surface varied between 0.005 to 0.01 μm [3]. Experimental studies indicated that Cl<sup>-</sup> and SO<sub>4</sub><sup>2-</sup> anions destroy the formed oxide film and SO<sub>4</sub><sup>2-</sup> anion introduces a more destructive effect [4–14].

\* Corresponding authors.

Hydrogen could be easily oxidized in fuel cells using different electrochemical techniques to produce electric power. The growth of the H<sub>2</sub> economy has faced some difficulties due to operative methods for H<sub>2</sub> generation besides the technology of storage and distribution [15,16]. For instance, Boddien et al. [17] indicated that the production of H<sub>2</sub> from suitable starting materials, such as H<sub>2</sub>O, at a relatively low temperature, is critical. Also, Principi et al. [18] reported for the time being the alternative methods for H<sub>2</sub> storage have reached enough ripeness for implementations since none of them has yet taken up all the technical challenges [19].

The substitution idea for H<sub>2</sub> generation comes from using certain active metals such as Zn [20–23], Al [4,5], or their alloys during the dissolution process in acidic or alkaline solutions. Wang et al. [24] reviewed a promising way for the H<sub>2</sub> generation when Al and Al's alloys reduced water or hydrocarbons to H<sub>2</sub>. Al–H<sub>2</sub>O reactions under either alkaline or neutral conditions are most used, but metal passivation is still the main problem. Recently, Abd El Wanees et al. [25] utilized some surfactants as controllers for H<sub>2</sub> production when Zn is allowed to be corroded in presence of dilute HCl. The oxides of such molecules are easily adsorbed on the Zn surface and form a barrier film that resists the corrosion process.

In addition, metals exploitation is identified to be an effective, user-friendly, and safe approach for both H<sub>2</sub> production and energy storage. The produced H<sub>2</sub> gas chaperon for the corrosion reaction was found to depend on different factors such as the solution composition, pH, inundation time, and temperature. Deyab [26] proved that the corrosion products on the metal surface can mitigate the H<sub>2</sub> production and the presence of an inhibitor could diminish the metallic area exposed to the attack.

Generally, the presence of an organic compound that contains hetero-atoms such as oxygen, sulfur, phosphorus, and nitrogen is considered an effective corrosion inhibitor [27–33]. Such a compound impedes the active dissolution of the metallic surface via the formation of an adsorbed protective cover that conserves the metal from the destructive effect of the medium. The inhibition efficiency was found to depend on the type of the attached hetero-atoms and decreases in the order P > S > N > O. The inhibition adequacy of some inhibitive molecules towards the corrosion of aluminum in acidic solution was found to depend on the nature and structure of the formed coat on the metal surface [34].

Hydrogen has received greater attention recently as an energy storage option, and the production of hydrogen is useful in the operation of the fuel cell. Controlling hydrogen production as clean nascent by using simple cheap chemicals, and therefore their economic feasibility is beneficial. Little work has been done on using dihydropyridine derivatives as corrosion inhibitors for steel in acid solutions [8,28,30]. In this study two compounds, namely, 2-oxo-1,2-dihydropyridine-3-carboxylic acid (ODCA) and 2-oxo-6-phenyl-1,2-dihydropyridine-3-carboxylic acid (OPDCA) were evaluated as inhibitors towards the destruction of Al<sub>2</sub>O<sub>3</sub> film and H<sub>2</sub> production on Al in 2.0 M HCl solutions. The adsorption and mechanism of action of such compounds were examined. The thermodynamic adsorption parameters  $\Delta G_{\text{ads}}^{\circ}$  and  $K_{\text{ads}}$  were deduced and discussed. The study was

evaluated by weight loss, open-circuit potential, gasometry, galvanostatic polarization, and electrochemical impedance spectroscopy (EIS), measurements complemented by surface investigation using a scanning electron microscopy (SEM).

## 2. Experimental set-up

### 2.1. Materials and methods

High-purity (99.98%) rectangular aluminum samples with dimensions of 2.5 cm × 4.0 cm × 0.4 cm were used for gravimetry and gasometry measurements. The procedure for sample preparation and measurement is like that described before [5]. For potential measurements, a rod of Al (used as a working electrode) was entrenched in epoxy resin with a free surface area of 0.34 cm<sup>2</sup>. Before each run, the surface of Al was abraded with the finest grade emery papers until reached a mirror finish, rinsed with acetone, and finally washed with distilled water. 2-Oxo-1,2-dihydropyridine-3-carboxylic acid (ODCA) and 2-oxo-6-phenyl-1,2-dihydropyridine-3-carboxylic acid (OPDCA) were obtained from Sigma-Aldrich (Merck) chemicals, Table 1. Experiments were executed at a constant temperature, 25°C ± 1°C, using an air thermostat.

### 2.2. Gravimetric measurements

The cleaned Al sheet was weighed (area = 24.45 cm<sup>2</sup>) before and after immersion in 100 mL of the test solution for the desired time. The average weight loss ( $\Delta m$ ) was determined for each run and the rate of corrosion,  $r_{\text{corr}}$ , was calculated using Eq. (1) [35]:

$$r_{\text{corr}} = \left( \frac{\Delta}{\text{time} \cdot \text{area}} \right) \quad (1)$$

The values of corrosion rates in the blank solution,  $r_{\text{free}}$  and in the inhibitive solutions,  $r_{\text{inh}}$ , were used to compute the surface coverage,  $\theta$  and the inhibition efficiency,  $\eta\%$  of the used inhibitors, according to Eqs. (2) and (3), respectively.

$$\theta = \left( 1 - \frac{r_{\text{inh}}}{r_{\text{free}}} \right) \quad (2)$$

$$\eta\% = \left( 1 - \frac{r_{\text{inh}}}{r_{\text{free}}} \right) 100 \quad (3)$$

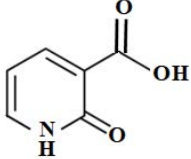
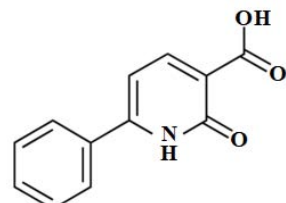
### 2.3. Open-circuit potential measurements

*E-t* curves were constructed by pursuing up the change in the potential of Al to the nearest mV, using Wenking potentiometer type PPT 70, and a reference electrode (SCE) until reaching a steady state,  $E_{\text{st}}$ . Each run was executed with a newly polished electrode surface immersed in a newly prepared solution.

### 2.4. Hydrogen evolution measurement

The system of gasometry and the procedure of measurements were like that described before [25]. The values

Table 1  
Inhibitor names, chemical structure, empirical formula, and molecular weight of the used inhibitors

Inhibitors name	Chemical structure	Empirical formula	Molecular weight
2-Oxo-1,2-dihydropyridine-3-carboxylic acid (ODCA)		C <sub>6</sub> H <sub>5</sub> NO <sub>3</sub>	139.11
2-Oxo-6-phenyl-1,2-dihydropyridine-3-carboxylic acid (OPDCA)		C <sub>12</sub> H <sub>9</sub> NO <sub>3</sub>	215.20

of surface coverage,  $q$  and inhibition efficiency,  $\eta''$ , were calculated from the values of corrosion rates,  $r'_{\text{inh}}$  and  $r'_{\text{free}}$  with and without inhibitors, respectively, according to Eqs. (5) and (6), respectively:

$$\theta = \left( 1 - \frac{r'_{\text{inh}}}{r'_{\text{free}}} \right) \quad (4)$$

$$\eta'' = \left( 1 - \frac{r'_{\text{inh}}}{r'_{\text{free}}} \right) 100 \quad (5)$$

### 2.5. Galvanostatic polarization measurements

The procedure for carrying the galvanostatic polarization and the construction of  $I$ - $E$  curves were like earlier studies [36]. A saturated calomel electrode, SCE, and Pt wire were used as a reference and a counter electrode, respectively.

### 2.6. Electrochemical impedance spectroscopy measurements

Electrochemical impedance spectroscopy (EIS) measurements were done using a Volta lab 80 (PGZ 402) potentiostat with Volta master 4 software. EIS curves were obtained by employing a frequency range of 100 kHz to 0.1 Hz using a signal amplitude of 10 mV using AC signals at open-circuit potential.

### 2.7. Scanning electron microscope investigation

The surface of some Al specimens was prepared and cleaned as usual. The surface morphology was investigated before and after inundation for a period of 2 h in 2.0 M HCl and 2.0 M HCl +  $1 \times 10^{-4}$  M OPDCA solutions. A scanning electron microscope, A Joel type, JSM-5410 (Japan), with an accelerated voltage of 25 kV and a working distance of 20 mm was used for surface investigations.

Table 2

Rate of corrosion,  $r'$ , mg/cm<sup>2</sup>-min, the surface coverage,  $\theta$ , and the inhibition efficiency,  $\eta\%$  at different concentrations of inhibitors, at 25°C

2.0 M HCl + inhibitor	ODCA			OPDCA		
	$r'$	$\theta$	$\eta\%$	$r'$	$\theta$	$\eta\%$
Free acid	0.411	–	–	0.411	–	–
$1 \times 10^{-5}$ M	0.333	0.190	19.0	0.316	0.231	23.1
$5 \times 10^{-5}$ M	0.295	0.282	28.2	0.274	0.333	33.3
$1 \times 10^{-4}$ M	0.245	0.404	40.4	0.226	0.450	45.0
$5 \times 10^{-4}$ M	0.167	0.594	59.4	0.141	0.656	65.6
$1 \times 10^{-3}$ M	0.104	0.747	74.7	0.088	0.786	78.6
$5 \times 10^{-3}$ M	0.084	0.796	79.6	0.066	0.840	84.0

## 3. Results and discussion

### 3.1. Gravimetric studies

The gravimetry method was used to calculate the corrosion rate,  $r$ , surface coverage,  $q$  and the inhibition efficiency,  $\eta\%$  (Table 2) for Al after inundation for 3 h. in 2.0 M HCl containing different additions of ODCA and OPDCA inhibitors, at 25°C. The increase of the inhibitor concentration decreases the rate of metal corrosion, while the surface coverage,  $q$  and the inhibition efficiency,  $\eta\%$  are increased due to an inhibitive effect. The inhibition efficiency reaches a maximum value of 84.0% and 79.6% with  $5 \times 10^{-3}$  M of OPDCA and ODCA inhibitors, successively. This could be attributed to the adsorption of such molecules on the metallic surface. Adsorption happens through non-bonding free electrons of N and O atoms of the inhibitor molecule as well as  $\pi$ -electrons of the aromatic ring. The higher inhibitive performance of OPDCA than ODCA inhibitors suggests a higher bonding ability of OPDCA molecules with the metallic surface, Table 2.

3.2. Open-circuit potential studies

The effect of the addition of ODCA and OPDCA inhibitors on the open-circuit potential,  $E$  of Al in 2.0 M HCl solutions were followed up at various inundation times. Fig. 1 depicts the  $E-t$  curves of Al in 2.0 M HCl solution devoid of and containing different amounts of ODCA inhibitor. Comparable curves were obtained with OPDCA inhibitor (curves not shown). The variation of the steady-state potential,  $E_{st}$  with  $\log C_{inh}$  of Al electrode is clarified in Fig. 2. The data of Figs. 1 and 2 expose the following:

- In free acid solution,  $E_{st}$  is reached from less negative values due to the destruction of pre-immersion formed  $Al_2O_3$  films and the continuous dissolution of the bare metal surface [5].
- The curves constructed of two featured segments before reaching  $E_{st}$  signalize the annihilation of the barrier  $Al_2O_3$  layer adjacent to the bare metal surface and the outer porous modulation on the Al surface.
- The duration required for the annihilation of the barrier oxide layer did not exceed more than the first 10 min of

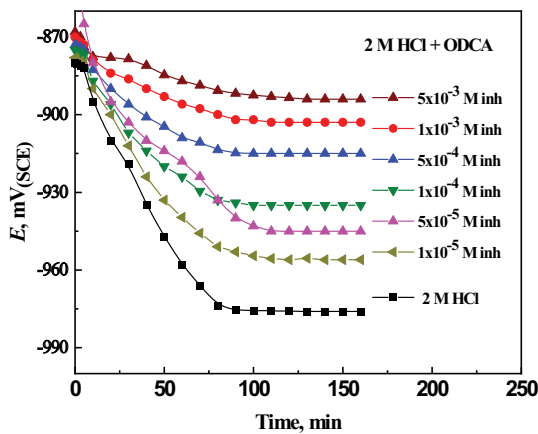


Fig. 1.  $E-t$  curves for Al in 2.0 M HCl solution devoid of and containing various additions of ODCA inhibitor, at 25°C.

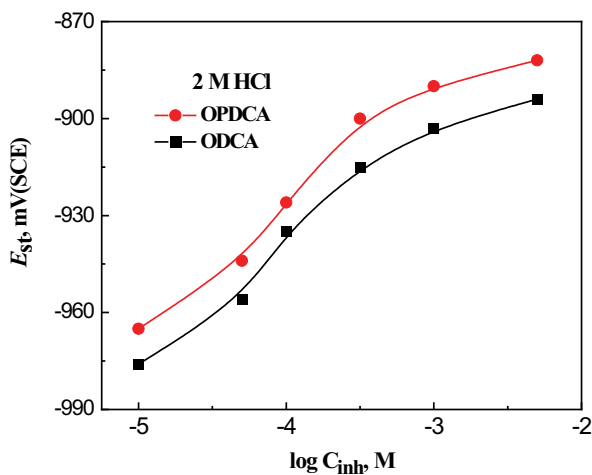


Fig. 2. Variation of  $E_{st}$  with  $\log C_{inh}$  for ODCA and OPDCA inhibitors on Al in 2.0 M HCl, at 25°C.

inundation and became stumpy with higher inhibitor addition. However, the annihilation of the outer porous modification took much time depending on the inhibitor type and concentration due to the simultaneous destruction of the porous-oxide layer and the bare metal surface [5].

- The addition of the ODCA and OPDCA inhibitors to a certain concentration shifts the potential of Al into a positive direction until reaching a steady state,  $E_{st}$ , which becomes less active the higher the additive concentration. Such behavior could be attributed to the decrease in the rate of metal destruction due to an adsorption step [5].
- Steady-state potential,  $E_{st}$ , varies with  $\log C_{inh}$  to give S-shaped curves (Fig. 2) confirming an adsorption process.

The curves in Fig. 3 depicted the  $E-\log t$  relation for Al in 2.0 M HCl solution devoid of and containing different concentrations of ODCA inhibitor. Comparable curves were obtained in the presence of an OPDCA inhibitor (curves not shown). The data of Fig. 3 and the like indicated two linear segments before reaching  $E_{st}$ , which was formerly attributed to the destruction of the inner and the outer  $Al_2O_3$  layers [37].

The variation of the open-circuit potential  $E$  with the logarithm of time,  $\log t$  follows the equation [38]:

$$E = a_1 - b_1 \log t \tag{6}$$

where  $a_1$  and  $b_1$  are constants that depend on the solution composition and the inspected material. It is noteworthy to see that the value of the constant  $b_1$  was diminished with increasing the inhibitor concentration illustrating the decrease in the rate of destruction of the  $Al_2O_3$  films with the concentration of the inhibitor.

Eq. 6 displayed that the rates of oxide film destruction, under the predominant experimental stipulations, follow a direct logarithmic law that is dependent on the additive concentration [33,39]. Such behavior depends mainly on the nature and properties of the  $Al_2O_3$  film formed on the metal surface.

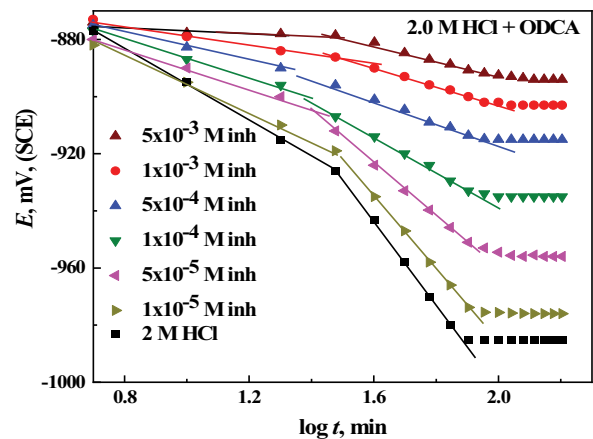


Fig. 3.  $E-\log t$  relation for Al in 2.0 M HCl solutions devoid of and containing different additions of ODCA inhibitor, at 25°C.

The rate of oxide film destruction can be determined by the relation [38]:

$$E = \text{const} \pm \left( \frac{2.303\delta^-}{\beta} \right) \log t \quad (7)$$

where  $\delta^-$  represents the rate of oxide film thickening or destruction in nm/unit decade in minutes and  $\beta = 58.5 \text{ nm/V}$  is a constant [5]. From the value of the slope,  $b_1$  of the linear part of  $E$ - $\log t$  curves (Fig. 3), the rate of oxide film destruction of the inner adherent,  $\delta_1^-$  and the outer porous,  $\delta_2^- \text{ Al}_2\text{O}_3$  modifications can be deduced [5,40], Table 3. Inspection of the data in this table emphasizes that:

- The rates of destruction of the duplex oxide films ( $\delta_1^-$  and  $\delta_2^-$ ) lessen with increasing the additions of ODCA and OPDCA. Such disposal could be attributed to the adsorption of the inhibitor molecules on the metallic surface [5].
- The presence of comparable concentrations of ODCA and OPDCA inhibitors decreased the rate of oxide film destruction in the order: OPDCA < ODCA.

Fig. 4A and B depict the variation of the rate of destruction of  $\delta_1^-$  and  $\delta_2^-$ , respectively, with the  $\log C_{\text{inh}}$  for ODCA and OPDCA inhibitors. It was found that  $\delta_1^-$  and  $\delta_2^-$  were decreased with increasing inhibitor concentration due to a suppression effect. The S-sigmoid nature of such curves could be confirmed by the adsorption nature of ODCA and OPDCA molecules on the metallic surface, lowering the destructive effect of HCl.

The surface coverage,  $\theta$ , and the percentage of inhibition efficiency,  $\eta\%$  of ODCA and OPDCA on Al in 2.0 M HCl can be determined from the rates of oxide-film destruction  $\delta_2^-$  [41].

$$\theta = \left[ 1 - \frac{\delta_2^-}{(\delta_2^-)^\circ} \right] \quad (8)$$

$$\eta\% = \left[ 1 - \frac{\delta_2^-}{(\delta_2^-)^\circ} \right] 100 \quad (9)$$

Table 3

Rate of oxide film destruction,  $\delta_1^-$  and  $\delta_2^-$ , nm/unit decade, surface coverage,  $\theta$ , and the inhibition efficiency,  $\eta\%$  of Al in 2.0 M HCl at different concentrations of inhibitors, at 25°C

2.0 M HCl + inh	ODCA				OPDCA			
	$\delta_1^-$	$\delta_2^-$	$\theta$	$\eta\%$	$\delta_1^-$	$\delta_2^-$	$\theta$	$\eta\%$
Free	1.609	3.752	–	–	1.609	3.752	–	–
$1 \times 10^{-5}$ M	1.211	2.950	0.214	21.4	1.052	2.780	0.259	25.9
$5 \times 10^{-5}$ M	0.844	2.600	0.307	30.7	0.665	2.476	0.340	34.0
$1 \times 10^{-4}$ M	0.762	2.100	0.440	44.0	0.545	1.951	0.480	48.0
$5 \times 10^{-4}$ M	0.633	1.050	0.720	72.0	0.487	0.825	0.780	78.0
$1 \times 10^{-3}$ M	0.434	0.903	0.759	75.9	0.289	0.544	0.855	85.5
$5 \times 10^{-3}$ M	0.169	0.506	0.865	86.5	0.058	0.128	0.966	96.6

where  $(\delta_2^-)^\circ$  and  $(\delta_2^-)$  are the rates of oxide film destruction of the outer oxide layer on the Al surface in 2.0 M HCl devoid of and containing inhibitor, respectively.

The data from Tables 3 and 4 revealed that:

- The surface coverage,  $q$  and inhibition efficiency,  $\eta'$  increase with inhibitor concentration and decrease with temperature.
- At  $5 \times 10^{-3}$  M of inhibitor concentration, the values of  $\eta'$  reach 86.5% and 96.6% in the case of ODCA and OPDCA, successively, at 25°C.
- The increase in the values of  $q$  and  $\eta'$  confirm the suppression effect of the used organic molecules towards the destruction of  $\text{Al}_2\text{O}_3$  and  $\text{H}_2$  production according to the order: OPDCA > ODCA.

### 3.3. Gasometric study

To estimate the inhibition effect of the used inhibitors towards the dissolution of Al in 2 M HCl, the shrinking in the volume of the evolved hydrogen ( $V$ ) was followed up with the inundation time,  $t$ . Fig. 5 clarifies  $V$ - $t$  curves of Al in 2 M HCl devoid of and containing different additions

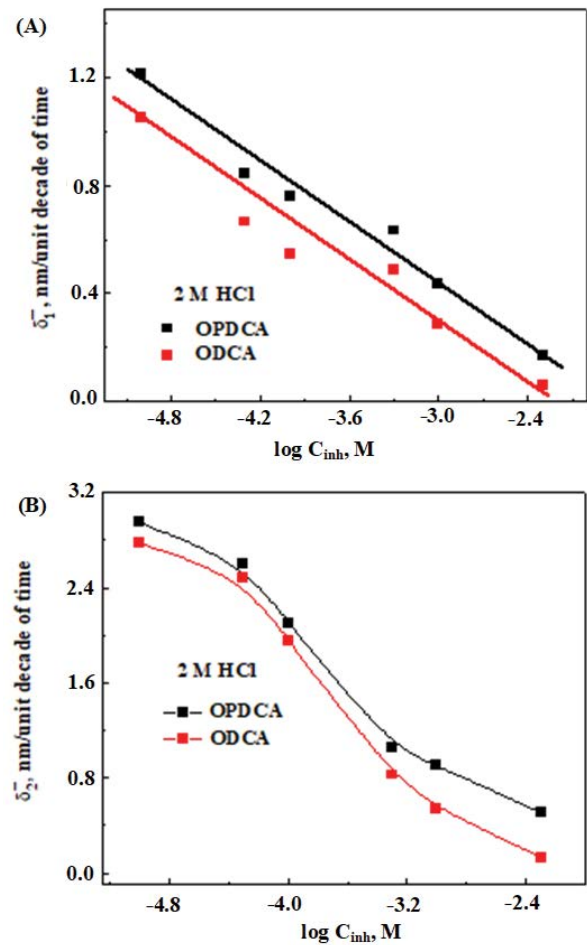


Fig. 4. Variation of the rate of destruction of  $\delta_1^-$  (A) and  $\delta_2^-$  (B), successively with  $\log C_{\text{inh}}$  for ODCA and OPDCA in 2.0 M HCl, at 25°C.

Table 4

Rate of oxide film destruction,  $\delta_2^-$ , nm/unit decade, surface coverage,  $\theta$ , and the inhibition efficiency,  $\eta\%$  of Al in 2.0 M HCl at various concentrations of inhibitors, at different temperatures

2.0 M HCl + inh	30°C			35°C			40°C		
	$\delta_2^-$	$\theta$	$\eta\%$	$\delta_2^-$	$\theta$	$\eta\%$	$\delta_2^-$	$\theta$	$\eta\%$
Free	4.050	–	–	4.400	–	–	4.750	–	–
2.0 M HCl + ODCA									
$1 \times 10^{-5}$ M	3.375	0.167	16.7	3.375	0.148	14.8	4.081	0.141	14.1
$5 \times 10^{-5}$ M	3.050	0.247	24.7	3.552	0.239	23.9	3.752	0.211	21.1
$1 \times 10^{-4}$ M	2.450	0.395	39.5	2.701	0.386	38.6	3.150	0.337	33.7
$5 \times 10^{-4}$ M	1.350	0.667	66.7	1.652	0.645	64.5	1.852	0.611	61.1
$1 \times 10^{-3}$ M	1.050	0.741	74.1	1.350	0.693	69.3	1.720	0.638	63.8
$5 \times 10^{-3}$ M	0.650	0.840	84.0	0.855	0.806	80.6	1.181	0.752	75.2
2.0 M HCl + OPDCA									
$1 \times 10^{-5}$ M	3.375	0.214	21.4	3.586	0.185	18.5	3.943	0.172	17.3
$5 \times 10^{-5}$ M	2.800	0.307	30.7	3.212	0.270	27.0	3.610	0.243	24.3
$1 \times 10^{-4}$ M	2.262	0.440	44.5	2.596	0.410	41.0	2.993	0.370	37.0
$5 \times 10^{-4}$ M	1.131	0.720	72.0	1.408	0.680	68.0	1.663	0.650	65.0
$1 \times 10^{-3}$ M	0.836	0.793	79.3	1.232	0.720	72.0	1.520	0.682	68.2
$5 \times 10^{-3}$ M	0.392	0.904	90.4	0.686	0.844	84.4	1.045	0.781	78.1

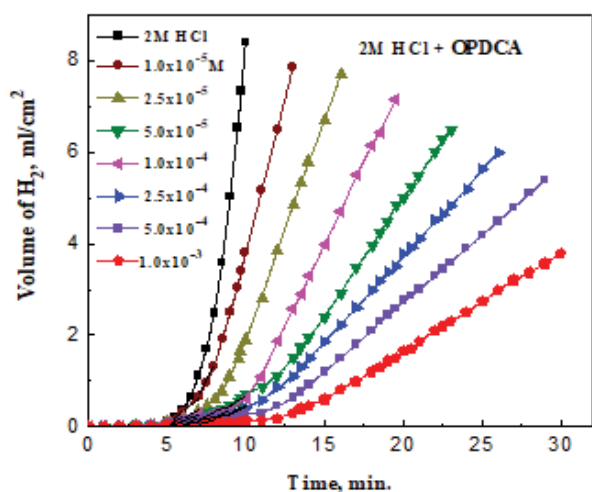
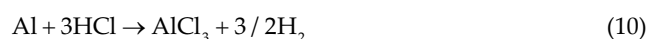


Fig. 5.  $V-t$  curves of Al in 2.0 M HCl devoid of and containing different additions of OPDCA inhibitor, at 25°C.

of OPDCA inhibitor, at 25°C. Comparable curves were obtained in presence of ODCA inhibitor (curves not shown). Inspection of the curves of Fig. 5 and the like discloses that the growth of  $H_2$  production starts after a narrow period of inundation of Al in the aggressive solution (within the first 6–12 min). This time is recognized as the induction period, which is the time required by the aggressive ions to spoilage the pre-immersion-formed oxide films and initiates the anodic and cathodic reactions [40]. The induction period increases with increasing the inhibitor concentration due to the delay of oxide film destruction in presence of the inhibitor. Such behavior is compatible with the time

taken for the destruction of the barrier oxide film by the potentiometric method.

However, after the induction time, the volume of the evolved  $H_2$  gas starts to increase linearly with the inundation time (Fig. 5) due to the contingent simultaneous destruction of the oxide film and the continual dissolution of the bare metal and liberating  $H_2$  according to the reaction:



As can be seen from Fig. 6 and the like, it is clear that the constringe in the produced volume of  $H_2$  gas by the presence of inhibitor can confirm the retardation of Al dissolution. The rate of the  $H_2$  production,  $r_{\text{corr}}$  can be determined from the slope of the linear part of the  $V-t$  relation, Table 5. The decrease in  $r_{\text{corr}}$  with inhibitor addition could be attributed to an inhibitive effect, due to the formation of an adsorbed inhibitor layer on the metal surface. On the other hand, the rise in solution temperature will diminish the induction period and increase  $r_{\text{corr}}$  due to an acceleration effect [28,42].

Fig. 6 portrays the variance in the rate of  $H_2$  production,  $r_{\text{corr}}$  with the logarithm of the inhibitor concentration,  $C_{\text{inh}}$ . The presence of sigmoid S-curves confirms the presence of an adsorption step during the inhibition process [33]. The values of  $q$  and  $\eta\%$ , Table 5, are increased with inhibitor concentration and take higher values with OPDCA than ODCA inhibitor.

### 3.4. Galvanostatic study

Fig. 7 depicts the anodic–cathodic galvanostatic polarization behavior ( $E-\log I$  curves) of Al in 2.0 M HCl devoid of and containing various concentrations of OPDCA

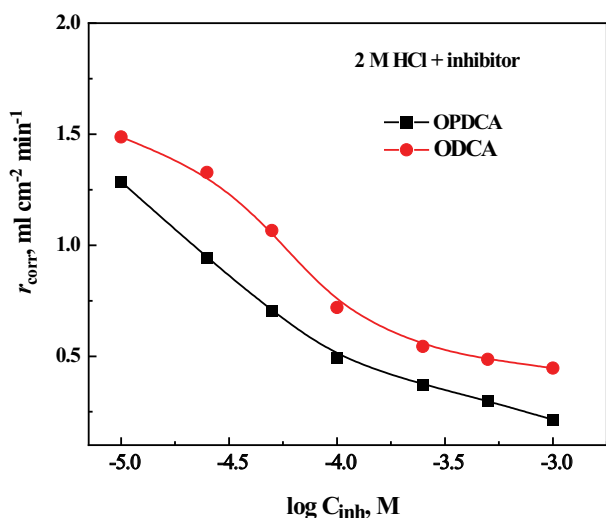


Fig. 6. Variation of the rate of  $H_2$  production,  $r_{corr}$  with the logarithm of the inhibitor concentration,  $C_{inh}$  at  $25^\circ C$ .

Table 5

Rate of corrosion,  $r_{corr}$ , surface coverage,  $\theta$ , and inhibition efficiency,  $\eta''$  for Al in presence of different concentrations of inhibitors (gasometry data)

HCl solution	ODCA			OPDCA		
	$r_{corr}$	$\theta$	$\eta''$	$r_{corr}$	$\theta$	$\eta''$
2 M	2.470	–	–	2.470	–	–
$1.0 \times 10^{-5}$ M	1.487	0.405	40.5	1.286	0.486	48.6
$2.5 \times 10^{-5}$ M	1.328	0.469	46.9	0.943	0.623	62.3
$5.0 \times 10^{-5}$ M	1.067	0.573	57.3	0.704	0.718	71.8
$1.0 \times 10^{-4}$ M	0.720	0.712	71.2	0.492	0.803	80.3
$2.5 \times 10^{-4}$ M	0.545	0.782	78.2	0.372	0.851	85.1
$5.0 \times 10^{-4}$ M	0.486	0.806	80.6	0.299	0.880	88.0
$1.0 \times 10^{-3}$ M	0.447	0.821	82.1	0.214	0.914	91.4

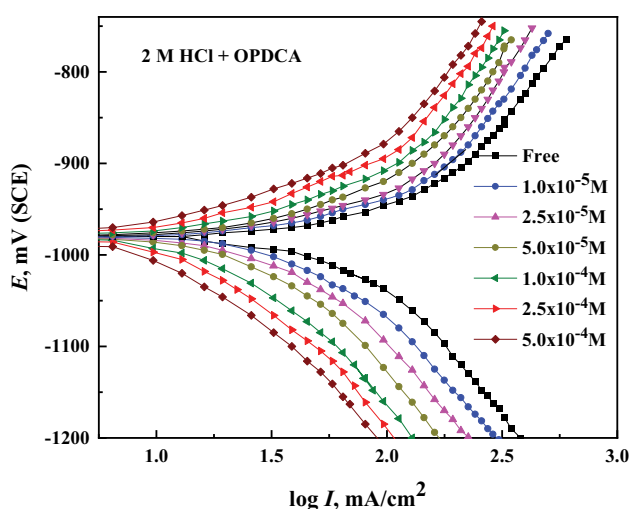


Fig. 7.  $E$ - $\log I$  curves of Al in 2.0 M HCl devoid of and containing various concentrations of OPDCA inhibitor, at  $25^\circ C$ .

inhibitor, at  $25^\circ C$ . Comparable curves are obtained in the case of ODCA (curves not shown). It is noted that each of the cathodic and anodic polarization curves is suppressed in presence of the inhibitor. Such behavior could occur due to the reduction in the corrosion rate as obvious from the convey of the cathodic curves to more negative values and the anodic ones to the more positive potentials. The reduction in the corrosion rate is due to the increase in the overvoltage accompanying the partial anodic and cathodic reactions, that is,  $Al_2O_3$  destruction and  $H_2$  production are under an activation-controlled process [43,44].

The electrochemical corrosion parameters, corrosion current density,  $I_{corr}$ , corrosion potential,  $E_{corr}$ , cathodic Tafel slope ( $\beta_c$ ), anodic Tafel slope ( $\beta_a$ ), surface coverage ( $\theta$ ), and percentage inhibition efficiency (IE%) are presented in Table 6.

The surface coverage ( $\theta$ ) and the inhibition efficiency (IE%) are calculated using the equations [35]:

$$\theta = \left( \frac{I_{corr}^{\circ} - I_{corr}}{I_{corr}^{\circ}} \right) \quad (11)$$

$$IE \% = \left( \frac{I_{corr}^{\circ} - I_{corr}}{I_{corr}^{\circ}} \right) 100 \quad (12)$$

where  $I_{corr}^{\circ}$  and  $I_{corr}$  are the uninhibited and inhibited corrosion current densities of Al in 2 M HCl, respectively. Inspection of the data of the curves of Fig. 7, as well as, the corrosion parameters recorded in Table 6 discloses the following:

- The non-significant changes in the values of  $\beta_a$  and  $\beta_c$ , besides the little displacement in  $E_{corr}$  (10–30 mV, SCE), which is <85 mV; provide that ODCA and OPDCA molecules behaved as mixed-type inhibitors [35,42].
- The corrosion potential ( $E_{corr}$ ) shifts slightly to a less negative direction, while the corrosion current density ( $I_{corr}$ ) is decreased with increasing the inhibitor concentration.
- As the inhibitor concentration is increased, the values of surface coverage ( $\theta$ ) and inhibition efficiency (IE%) are markedly increased, supporting the inhibitive effect of ODCA and OPDCA molecules towards the corrosive effect of HCl on Al surface.
- At a comparable concentration,  $\theta$  and IE% increase in the order: ODCA < OPDCA, which is the same order obtained by other techniques.

### 3.5. Electrochemical impedance spectroscopy study

EIS measurements are carried out at  $25^\circ C$  in 2.0 M HCl without and with ODCA and OPDCA inhibitors. Fig. 8 depicts the Nyquist plots for Al in 2.0 M HCl solution without and with different concentrations of OPDCA inhibitor. Similar curves are obtained with ODCA inhibitor (curves are not shown). As shown from this figure and the like, the impedance spectra consist of a large capacitive loop at high frequencies is usually related to charge transfer resistance of the dissolution process and the double layer behavior, and the inductive loop may be attributed to the relaxation processes in the passive oxide film covering the

Table 6

Corrosion potential,  $E_{corr}$ , corrosion current,  $I_{corr}$ , anodic Tafel slope,  $\beta_a$ , cathodic Tafel slope,  $\beta_c$ , surface coverage,  $\theta$ , and the inhibition efficiency, IE% for Al in 2.0 M HCl, at 25°C

Conc., M	$-E_{corr}$ , mV	$I_{corr}$ , mA/m <sup>2</sup>	$\beta_a$ , mV/decade	$\beta_c$ , mV/decade	$\theta$	IE%
2.0 M HCl	983	810	128	255	–	–
2.0 M HCl + ODCA						
$1.0 \times 10^{-5}$ M	977	53.2	155	265	0.343	34.3
$2.5 \times 10^{-5}$ M	975	38.7	158	270	0.522	52.2
$5.0 \times 10^{-5}$ M	972	30.8	165	275	0.620	62.0
$1.0 \times 10^{-4}$ M	968	25.6	169	276	0.684	68.4
$2.5 \times 10^{-4}$ M	964	17.5	172	279	0.784	78.4
$5.0 \times 10^{-4}$ M	961	12.3	174	285	0.848	84.8
2.0 M HCl + OPDCA						
$1.0 \times 10^{-5}$ M	976	52.5	170	346	0.352	35.2
$2.5 \times 10^{-5}$ M	974	36.4	177	354	0.551	55.1
$5.0 \times 10^{-5}$ M	971	26.7	194	390	0.671	67.1
$1.0 \times 10^{-4}$ M	966	19.8	196	399	0.756	75.6
$2.5 \times 10^{-4}$ M	961	14.2	202	398	0.825	82.5
$5.0 \times 10^{-4}$ M	959	10.1	204	400	0.875	87.5

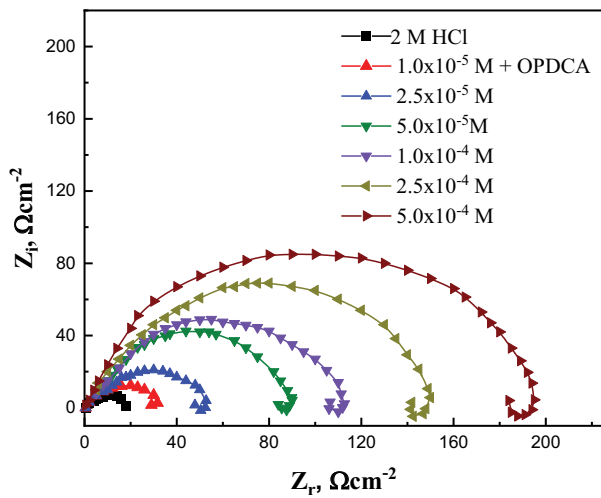


Fig. 8. Nyquist plots of Al in 2.0 M HCl devoid of and containing various concentrations of OPDCA inhibitor, at 25°C.

metal surface [45] or related to stabilization of a film formed by the adsorbed inhibitor molecules [46]. Also, the similarities between the Nyquist curves in both the blank and the inhibitor solutions point to the similarity in the mechanism of dissolution of Al metal in the absence and presence of inhibitors [47].

In addition, the depressed form of the higher frequency loop reflects the surface inhomogeneity of structural or interfacial origin, such as those found in the adsorption process [48]. EIS parameters of these loops were fitted with an electrical equivalent circuit as displayed in Fig. 9, where  $R_s$  is the solution resistance,  $R_{ct}$  is the charge transfer resistance related to the OCP corrosion reaction, while the CPE represents a constant phase element related to the

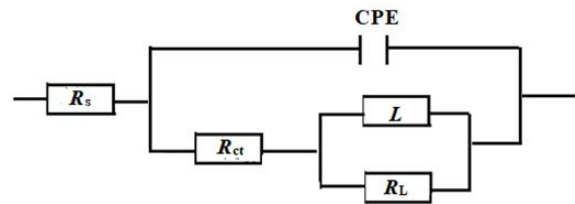


Fig. 9. Equivalent circuit model that used for fitting the experimental results.

non-ideal capacity ( $C_{dl}$ ),  $R_L$  and  $L$  represent the inductive elements [49].

The EIS parameters obtained from the Al are listed in Table 2. It is clear that the increase in  $R_{ct}$  with the inhibitor concentration, besides the decrease in  $C_{dl}$  points to the inhibition influence of such inhibitors. The surface coverage,  $\theta$ , and the inhibition efficiency (IE%) were calculated using the following equations [25,35].

$$\theta = \left( \frac{R_{ct} - R_{ct}^0}{R_{ct}} \right) \tag{13}$$

$$IE\% = \left( \frac{R_{ct} - R_{ct}^0}{R_{ct}} \right) 100 \tag{14}$$

where  $R_{ct}$  is the charge transfer resistance with inhibitor and  $R_{ct}^0$  is the charge transfer resistance without inhibitor. According to Table 7, it can be concluded that with an increase in the inhibitor concentration of OPDCA and ODCA, there was an increase in the charge transfer resistance. In contrast, the values of the double layer ( $C_{dl}$ ) dropped rapidly with an increase in the concentration of the inhibitor suggesting that



Table 7

Impedance parameters,  $R_p$ ,  $\Omega/\text{cm}^2$ ,  $C_{dl}$ ,  $\mu\text{F}/\text{cm}^2$ , surface coverage,  $\theta$ , and the inhibition efficiency,  $IE'$ , % for Al in 2.0 M HCl, at 25°C

Concentration, M	OPDCA				ODCA			
	$R_p$ , $\Omega/\text{cm}^2$	$C_{dl}$ , $\mu\text{F}/\text{cm}^2$	$\theta$	$IE'$ , %	$R_p$ , $\Omega/\text{cm}^2$	$C_{dl}$ , $\mu\text{F}/\text{cm}^2$	$\theta$	$IE'$ , %
2.0 M HCl	3.8	214	–	–	3.8	214	–	–
$1.0 \times 10^{-5}$ M	5.9	138.3	0.356	35.6	5.75	141.9	0.339	33.9
$2.5 \times 10^{-5}$ M	8.6	78.7	0.558	55.8	8	84.6	0.525	52.5
$5.0 \times 10^{-5}$ M	11.6	43.4	0.672	67.2	10.1	49.8	0.624	62.4
$1.0 \times 10^{-4}$ M	15.3	30.1	0.752	75.2	12.1	26.2	0.686	68.6
$2.5 \times 10^{-4}$ M	21.7	20.5	0.825	82.5	17.3	25.8	0.783	78.3
$5.0 \times 10^{-4}$ M	31.7	12.2	0.88	88.0	25.5	15.1	0.85	85.0

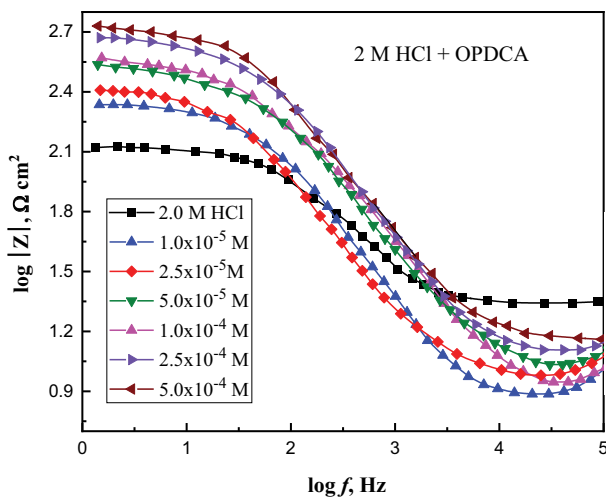


Fig. 10. Bode plots of Al in 2.0 M HCl devoid of and containing various concentrations of OPDCA inhibitor, at 25°C.

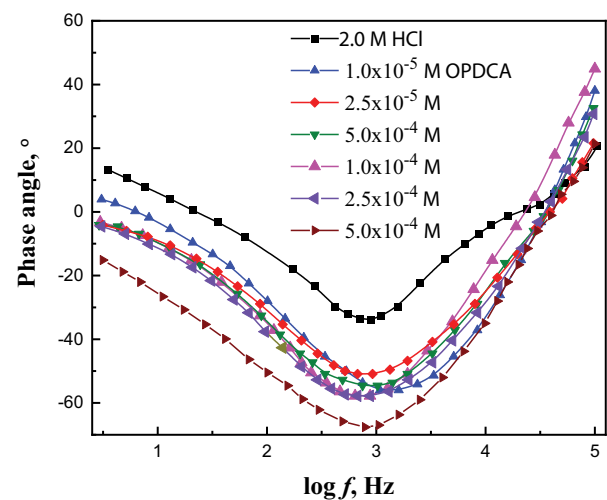


Fig. 11. Phase angle plots of Al in 2.0 M HCl devoid of and containing various concentrations of OPDCA inhibitor, at 25°C.

the water molecules adsorbed on the surface of Al surface were replaced by molecules of the added inhibitor, with a lower dielectric constant according to the Helmholtz model equation, as follows: The decrease of the  $C_{dl}$  value reflects an increase in the double layer thickness, which indicates the possibility of formation of protective film on the Al surface by an adsorption process [25,47].

Figs. 10 and 11 show the Bode and phase angle plots of the Al electrode, successively, with various concentrations of OPDCA inhibitor in 2.0 M HCl, at 25°C. These plots point to the exact frequency at which the data points are recorded. As the concentration of the inhibitor increased, the phase angle plots became wider in the high-frequency range, which indicates that the corrosion inhibition of Al was enhanced due to the increase in the inhibitor coverage on the Al surface. Also, the impedance modulus was the highest at the concentration of  $5 \times 10^{-4}$  M, indicating the high efficiency of the adsorption of the used inhibitors at the Al surface. This demonstrates that there was better protection against corrosion in the corrosive HCl medium to reach 88% and 85% in the case of  $5 \times 10^{-4}$  M of OPDCA and ODCA, successively, at 25°C. The results obtained from the EIS measurements are in good agreement with those obtained from other experimental techniques.

### 3.6. Effect of temperature

The effect of temperature on the rate of destruction of the outer porous  $\text{Al}_2\text{O}_3$  layer ( $\delta_2^-$ ) in 2.0 M HCl with and without different concentrations of ODCA and OPDCA inhibitors was further examined, at a temperature range of 298–313 K. The constructed  $E$ - $\log t$  curves at different temperatures were used to calculate  $\delta_2^-$ , Table 4. It was found that  $\delta_2^-$  was increased with raising the solution temperature, which is consistent with the theoretical expectation that the corrosion process should increase with temperature [34,51].

The apparent activation energy,  $E_a$ , for oxide film destruction of the outer porous  $\text{Al}_2\text{O}_3$  layer,  $\delta_2^-$  in 2.0 M HCl devoid of and containing different concentrations of inhibitors can be computed using the equation [34,51]:

$$\delta_2^- = A \exp\left(\frac{-E_a}{RT}\right) \quad (15)$$

where  $A$  symbolizes the Arrhenius factor,  $R$  is the universal gas constant (8.314 J/mol) and  $T$  is the absolute temperature. The relation between  $\log \delta_2^-$  and  $T^{-1}$  for Al in 2.0 M HCl in presence of different concentrations of ODCA can be plotted

in Fig. 12. The values of  $E_a$  for the destruction of the porous  $Al_2O_3$  layer are given in Table 8. The value of  $E_a$  in free acid solution is found to be 12.26 kJ/mol. In presence of inhibitors,  $E_a$  varies between 16.75 and 77.40 kJ/mol, depending on the inhibitor type and its concentration. The increase in activation energy  $E_a$  refers to the retardation of the rate of oxide film destruction due to the adsorption of the inhibitor molecules on the metallic surface forming a protective film [30]. Moreover, the increase in  $E_a$  values supports the physisorption mechanism [25]. The values of  $\delta_2^-$  (nm/unit decade) are used to locate the values of apparent enthalpy of activation ( $\Delta H_a$ ) and apparent entropy of activation

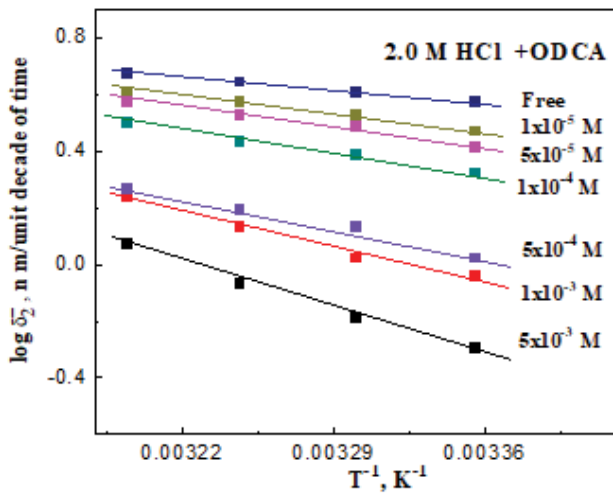


Fig. 12. Arrhenius plots ( $\log \delta_2^-$  against  $T^{-1}$ ) for Al in 2.0 M HCl in the absence and presence of different concentrations of ODCA.

Table 8

Linear correlation coefficient,  $r^2$ , activation energy,  $E_a$ , enthalpy,  $\Delta H_a$ , and entropy,  $\Delta S_a$ , for Al in 2.0 M HCl without and with ODCA and OPDCA inhibitors

Concentration, M	$r^2$	$E_a$ , kJ/mol	$\Delta H_a$ , kJ/mol	$-\Delta S_a$ , kJ/mol
2.0 M HCl	0.990	12.26	09.72	202
2.0 M HCl + ODCA				
$1.0 \times 10^{-5}$ M	0.999	16.75	14.23	188
$5.0 \times 10^{-5}$ M	0.999	18.55	16.02	184
$1.0 \times 10^{-4}$ M	0.999	20.37	17.84	179
$5.0 \times 10^{-4}$ M	0.989	28.70	26.17	157
$1.0 \times 10^{-3}$ M	0.999	33.81	31.29	141
$5.0 \times 10^{-3}$ M	0.978	43.66	41.11	113
2.0 M HCl + ODCA				
$1.0 \times 10^{-5}$ M	0.993	18.20	5.63	18/8
$5.0 \times 10^{-5}$ M	0.999	19.70	17.17	183
$1.0 \times 10^{-4}$ M	0.981	22.00	19.52	178
$5.0 \times 10^{-4}$ M	0.977	36.00	33.55	156
$1.0 \times 10^{-3}$ M	0.999	53.90	51.40	141
$5.0 \times 10^{-3}$ M	0.987	77.40	74.82	112

( $\Delta S_a$ ) for the destruction of the porous  $Al_2O_3$  film, using the transition state equation [52]:

$$\frac{\delta_2^-}{T} = \frac{R}{Nh} \exp\left(\frac{\Delta S_a}{RT}\right) \exp\left(\frac{-\Delta H_a}{RT}\right) \quad (16)$$

where  $N$  is Avogadro's number and  $h$  is Planck's constant. Eq. (16) can be represented as a variation between ( $\log \delta_2^- T^{-1}$ ) against  $T^{-1}$ , Fig. 13. The values of  $\Delta H_a$  and  $\Delta S_a$  were calculated and represented in Table 8. The positive sign of  $\Delta H_a$  reflects the endothermic nature of the destruction process in the case of blank and inhibitor solutions [53]. The increase in the values of  $\Delta H_a$  in presence of the inhibitor means that the destruction of the  $Al_2O_3$  film becomes more difficult in presence of ODCA and OPDCA inhibitors [54]. The negative sign of  $\Delta S_a$  (Table 8) indicates a decrease in the disorder of the rate-determining step of the activated complex during the transition from reactant to the activated complex [55,56].

### 3.7. Adsorption isotherm

Various adsorption isotherms are attempted to fit the surface coverage,  $\theta$ , including that of Temkin, Frumkin, Langmuir, and Freundlich isotherms. Experimental data was found to fit the Langmuir adsorption isotherm. The surface coverage,  $\theta$  was calculated at different concentrations of OPDCA and ODCA, from the values of  $\delta_2^-$ , Eq. (8). The surface coverage,  $\theta$ , is related to the inhibitor concentration,  $C_{inh}$  by the equation [35]:

$$\frac{C_{inh}}{\theta} = \frac{1}{k_{ads}} + C_{inh} \quad (17)$$

where  $K_{ads}$  is the equilibrium constant of the adsorption-desorption process, and  $C_{inh}$  is the inhibitor concentration. Fig. 14A and B represent a plot of  $C_{inh} \theta^{-1}$  against  $C_{inh}$  for ODCA and OPDCA inhibitors, respectively, at different temperatures. The plots fit straight-line relations with

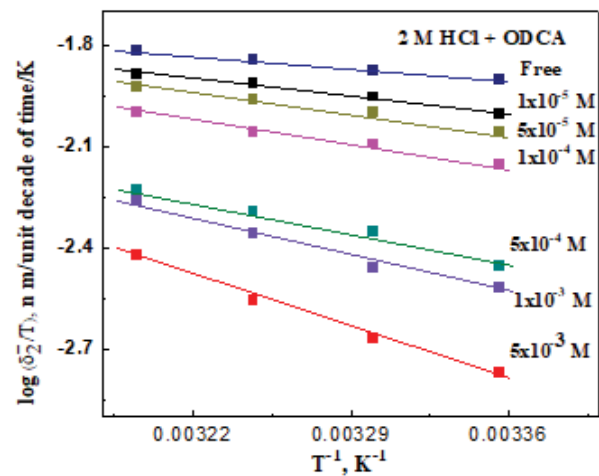


Fig. 13. Transition state plots ( $\log \delta_2^-$  against  $T^{-1}$ ) for Al in 2.0 M HCl in the absence and presence of different concentrations of ODCA.

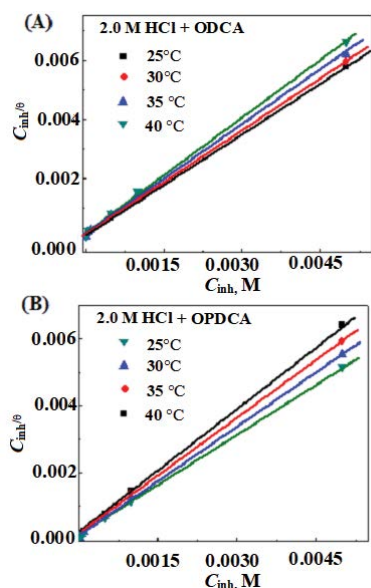


Fig. 14. Langmuir adsorption isotherms for ODCA (A) and OPDCA (B), respectively, on the Al surface in 2.0 M HCl, at different temperatures.

Table 9

Values of the linear correlation coefficient,  $r^2$ , slope, intercept, and  $K_{ads}$  for adsorption of inhibitors on Al in 2 M HCl, at different temperatures

Inhibitor	Temp., K	$r^2$	Slope	Intercept $\times 10^4$	$K_{ads}$ mol/L
ODCA	288	0.990	1.14	1.58	6297
	293	0.998	1.16	1.82	5278
	298	0.994	1.21	2.13	4493
	303	0.999	1.27	2.44	3525
OPDCA	288	0.989	1.01	1.35	7363
	293	0.999	1.07	1.71	5848
	298	0.988	1.14	2.00	5000
	303	0.993	1.21	2.36	4237

slopes close to unity and with a strong correlation coefficient ( $r^2 > 0.99$ ), Table 8. The adsorption–desorption equilibrium constant ( $K_{ads}$ ) can be deduced from the reciprocal of the intercept of  $C_{inh}^0$  vs.  $C_{inh}$  plots, Fig. 14A and B. The calculated values of  $K_{ads}$  are found to be 6,297 and 7,363 mol/L for ODCA and OPDCA, respectively, at 25°C Table 9. These values are slightly lowered with temperature, Table 9. However, the higher values of  $K_{ads}$  indicate a strong adsorption capacity of ODCA and OPDCA inhibitors on the metallic surface [34].

The values of  $K_{ads}$  (Table 9) are used to calculate the free energy of adsorption,  $\Delta G_{ads}^\circ$  for ODCA and OPDCA on the Al surface using Eq. (18) [35]:

$$k_{ads} = \frac{1}{55.5} \exp\left(\frac{\Delta S_{ads}^\circ}{RT}\right) \quad (18)$$

where  $R$  is the universal gas constant and 55.55 is the molar concentration of  $H_2O$  in mol/L.  $\Delta G_{ads}^\circ$  values are calculated

Table 10

Standard thermodynamic adsorption parameters,  $\Delta G_{ads}^\circ$ ,  $\Delta H_{ads}^\circ$ , and  $\Delta S_{ads}^\circ$  for ODCA and OPDCA inhibitors on Al in 2.0 M HCl, at different temperatures

Inhibitor	Temp., K	$\Delta G_{ads}^\circ$ kJ/mol	$\Delta H_{ads}^\circ$ kJ/mol	$\Delta S_{ads}^\circ$ J/mol·K
ODCA	288	30.56		28.1
	293	30.66	-22.46	28.0
	298	30.79		27.9
	303	30.69		27.2
288	30.94	9.60		
OPDCA	293	30.91	-28.17	9.40
	298	31.05		9.70
	303	31.16		9.90

to be -30.66 and -30.91 kJ/mol for ODCA and OPDCA, successively, at 25°C, Table 10. The negative value of  $\Delta G_{ads}^\circ$  indicates the spontaneous adsorption process of ODCA and OPDCA inhibitors on the Al surface and the stability of the adsorbed layer.

In general,  $\Delta G_{ads}^\circ$  values of -20 kJ/mol or less negative are related to the physisorption, on account of electrostatic attractions between inhibitor molecules and the metal surface [34]. On the other hand,  $\Delta G_{ads}^\circ$  values of -40 kJ/mol or more negative encompass charge transfer from the inhibitor molecule to the metallic surface to form a coordinate covalent bond [34]. In our study, the  $\Delta G_{ads}^\circ$  values for adsorption of ODCA and OPDCA on the Al surface, successively, varied between -30.56 and -31.16 kJ/mol, that is, the adsorption mechanism comprises mixed-type interactions, including physisorption and chemisorption types [35].

Generally, it is known that the adsorption thermodynamic parameters are used to illustrate the adsorption behavior of ODCA and OPDCA inhibitors on the Al surface. The standard enthalpy of adsorption,  $\Delta H_{ads}^\circ$  can be computed from Van't Hoff equation [55,56].

$$\frac{dK_{ads}}{dT} = \frac{\Delta H_{ads}^\circ}{RT^2} \quad (19)$$

where  $R$  is the gas constant (8.314 J/mol·K) and  $T$  is the absolute temperature (K). The indefinite integration of Eq. (19) can give:

$$\ln K_{ads} = \left(\frac{-\Delta H_{ads}^\circ}{RT}\right) + \text{constant} \quad (20)$$

Fig. 15 depicts the variation of  $\ln K_{ads}$  vs.  $1/T$ . Straight lines with slopes equal to  $-\Delta H_{ads}^\circ/R$  are obtained. The calculated  $\Delta H_{ads}^\circ$  values are found to be -22.46 and -28.17 kJ/mol for ODCA and OPDCA, successively, Table 10. The endothermic adsorption process ( $\Delta H_{ads}^\circ > 0$ ) is accompanied by the chemisorption process, while the exothermic one ( $\Delta H_{ads}^\circ < 0$ ) may be accompanied by physisorption, chemisorption, or a mixture of the two [25]. In our case, the negative sign of  $\Delta H_{ads}^\circ$  indicates the exothermic nature of the adsorption of

ODCA and OPDCA on the Al surface in HCl. On another side, the value of enthalpy is  $<41.8$  kJ/mol, which announces that the adsorption of ODCA and OPDCA on the Al surface is not merely physical or chemical, but a mixed type.

The standard adsorption of entropy,  $\Delta S_{\text{ads}}^{\circ}$ , can be obtained from the relation [57]:

$$\Delta H_{\text{ads}}^{\circ} = \left( \frac{\Delta H_{\text{ads}}^{\circ} - \Delta G_{\text{ads}}^{\circ}}{T} \right) \quad (21)$$

The values of  $\Delta S_{\text{ads}}^{\circ}$  can be calculated and collected in Table 10. The positive values of  $\Delta S_{\text{ads}}^{\circ}$  confirm that the adsorption is accompanied by an increase in the disordered system due to the adsorption of inhibitor molecules on the metallic surface [58].

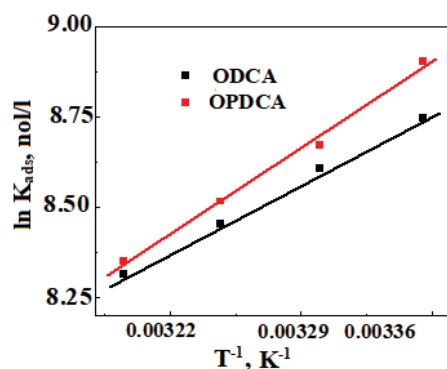


Fig. 15. Variation of  $\ln K_{\text{ads}}$  vs.  $1/T$  for ODCA and OPDCA on Al in 2.0 M HCl.

### 3.8. Surface morphology

SEM technique was employed to further prove the ability of the used inhibitors to protect the surface of Al samples from the corrosive influence of HCl. Fig. 16A exhibits the SEM micrograph of the polished Al surface before immersion in the 2.0 M HCl solution. It displays a smooth appearance with some scratching lines due to the mechanical polishing process. In contrast in the absence of an inhibitor, the effect of HCl on the polished Al sample after immersion for 2 h in the aggressive solution destroy the Al sample leaving a rough surface covered with a huge amount of deep cracks and large holes, Fig. 16B. This behavior suggests strong damage and a severe dissolution of Al metal in contact with 2.0 M HCl solution. The protective effect of the PODCA inhibitor appears strikingly, Fig. 16C. The destructive effect of HCl on the Al surface is highly mitigated. The surface of the investigated specimen appears with a less destructive effect and is covered by corrosion products. This may be accounted for a protective effect of PODCA on the Al surfaces reducing the metal dissolution.

### 3.9. Inhibition mechanism

Several experimental techniques such as potentiometry, gravimetry, gasometry, and galvanostatic have been done to illustrate the behavior of ODCA and OPDCA as inhibitors towards the corrosion of Al and to control the  $\text{H}_2$  production in HCl solutions. Generally,  $\text{Cl}^-$  ions can be easily adsorbed on the metallic surface to form  $(\text{AlCl})_{\text{ads}}$  [59]. The adsorption of ODCA and OPDCA molecules on the Al surface can be explicated by physical or/and chemisorption mechanisms. These molecules are organic bases; in presence of HCl

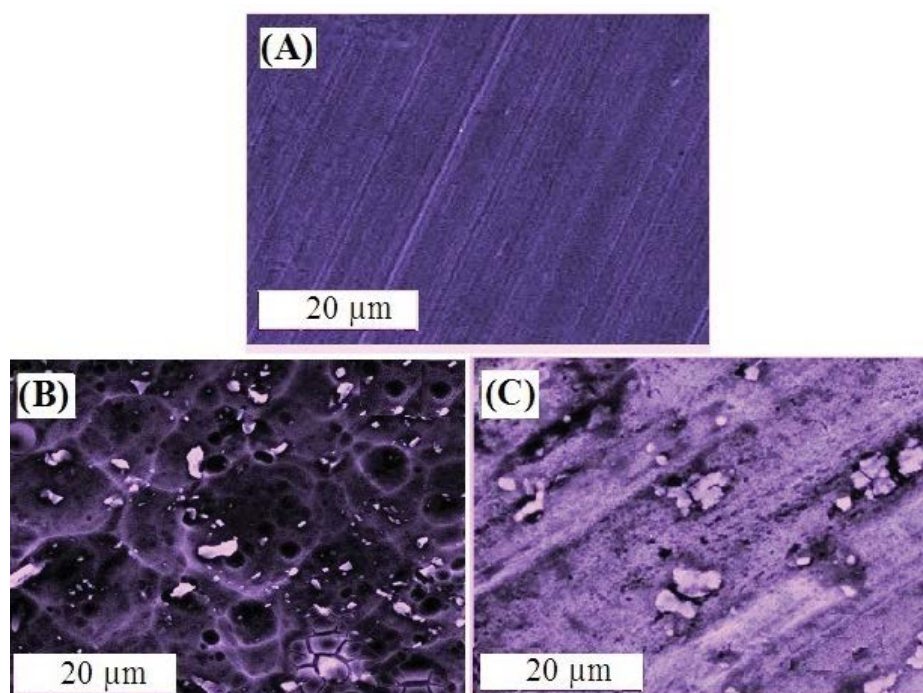


Fig. 16. Scanning electron micrographs of the polished Al surface before inundation in the aggressive solutions (A), after inundation for 2 h in 2.0 M HCl devoid of (B) and containing  $1 \times 10^{-4}$  M of OPDCA inhibitor (C).

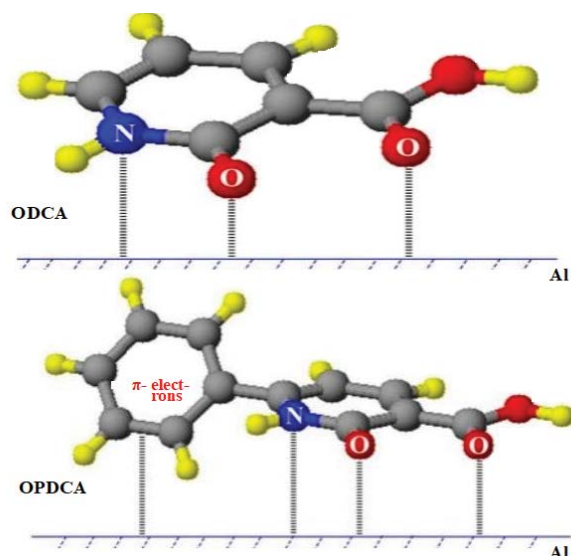


Fig. 17. Suggested adsorption model for ODCA and OPDCA molecules on Al surface.

behave as protonated or neutral forms. The adsorbed film shields the Al metal from the corrosive medium. Therefore, these inhibitors can tolerate the  $H_2$  production reactions, due to the electrostatic attraction with the active cathodic sites on the metallic surface. The free lone pairs of electrons located on O and N atoms (in ODCA and OPDCA) as well as the  $\pi$  electrons of the aromatic rings (in OPDCA) can reduce the partial anodic reaction of the metallic surface, due to adsorption on the active anodic sites. Moreover, the higher inhibition efficiency of OPDCA could be correlated to the bonding of  $\pi$  electrons of the aromatic ring with the metallic surface beside the high molecular weight to facilitate the adsorption process. OPDCA is thought to be adsorbed on the metal surface through different four sites, while ODCA molecules can be suggested to adsorb through only three active adsorption sites (Fig. 17).

#### 4. Conclusion

- ODCA and OPDCA molecules acted as good inhibitors towards the destruction of the  $Al_2O_3$  corrosion Al in 2 M HCl, and  $H_2$  production.
- The inhibition process is confirmed by the adsorption process according to Langmuir's model.
- The predominance of mixed chemical and physical adsorption was suggested based on thermodynamic parameters.
- The higher values of  $K_{ads}$  and the negative values of  $\Delta G_{ads}^\circ$  indicate a spontaneous strong adsorption process.
- Galvanostatic polarization data revealed a mixed type of process.

#### Acknowledgments

The authors express their gratitude to Princess Nourah bint Abdulrahman University Researcher supporting project number (PNURSP2023R53). Princess Nourah bint Abdulrahman University, Riyadh, Saudi Arabia.

#### References

- [1] H. Takahashi, M. Nagayama, Electrochemical behavior and structure of anodic oxide films formed on aluminum in a neutral borate solution, *Electrochim. Acta*, 23 (1978) 279–286.
- [2] H.H. Uhlig, R.W. Revie, *Corrosion and Corrosion Control: An Introduction to Corrosion Science and Engineering* (Third ed.), John Wiley & Sons, NY, 1981, pp. 69–73, 181–190, 341–354.
- [3] M.F. Lorking, J.E.O. Mayne, The corrosion of aluminum, *J. Appl. Chem.*, 11 (1961) 170–180.
- [4] A.M. Abdel-Gaber, B.A. Abd-El-Nabey, I.M. Sidahmed, A.M. El-Zayady, M. Saadawy, Kinetics and thermodynamics of aluminum dissolution in 1.0 M sulphuric acid containing chloride ion, *Mater. Chem. Phys.*, 98 (2006) 291–297.
- [5] S.M. Abd El Haleem, S. Abd El Wanees, E.E. Abd El Aal, A. Farouk, Factors affecting the corrosion behavior of aluminum in acid solutions. I. Nitrogen and/or sulfur-containing organic compounds as corrosion inhibitors for Al in HCl solutions, *Corros. Sci.*, 68 (2013) 1–13.
- [6] E.E. Abd El Aal, S. Abd El Wanees, A. Diab, S.M. Abd El Haleem, Environmental factors affecting the corrosion behavior of reinforcing steel III. Measurement of pitting corrosion currents of steel in  $Ca(OH)_2$  solutions under natural corrosion conditions, *Corros. Sci.*, 68 (2013) 1–13.
- [7] M. Abdallah, I.A. Zaafarany, S. Abd El Wanees, R. Assi, Breakdown of passivity of nickel electrode in sulfuric acid and its inhibition by pyridinone derivatives using the galvanostatic polarization technique, *Int. J. Corros. Scale Inhib.*, 4 (2015) 338–352.
- [8] M. Abdallah, I.A. Zaafarany, S. Abd El Wanees, R. Assi, Corrosion behavior of nickel electrode in NaOH solution and its inhibition by some natural oils, *Int. J. Electrochem. Sci.*, 9 (2014) 1071–1086.
- [9] S.M. Abd El Haleem, S. Abd El Wanees, Passivation of nickel in NaOH solutions, *Prot. Met. Phys. Chem. Surf.*, 54 (2018) 859–865.
- [10] A. Al-Gorair, A. Fawzy, H. Hawsawi, M. Sobhi, A. Alharbi, R.S. Abdel Hameed, S. Abd El Wanees, M. Abdallah, Evaluation of the anticorrosion and adsorption properties of polyethylene glycol and polyvinyl alcohol for corrosion of iron in 1.0 M NaCl solution, *Int. J. Electrochem. Sci.*, 16 (2021) 211119, doi: 10.20964/2021.11.03.
- [11] S.M. Abd El Haleem, S. Abd El Wanees, A.B. Radwan, Environmental factors affecting the corrosion behaviour of reinforcing steel. V. Role of chloride and sulphate ions in the corrosion of reinforcing steel in saturated  $Ca(OH)_2$  solutions, *Corros. Sci.*, 57 (2013) 1–15.
- [12] S. Abd El Wanees, A.S. Al-Gorair, H. Hawsawi, M.T. Alotaibi, M.G.A. Saleh, Inhibition of pitting corrosion of C-steel in oilfield-produced water using some purine derivatives, *Desal. Water Treat.*, 269 (2022) 21–32.
- [13] S. Abd El Wanees, M.M. Kamel, S.M. Rashwan, Y. Atef, M.G. Abd El Sadek, Initiation and inhibition of pitting corrosion on C-steel in oilfield-produced water under natural corrosion conditions, *Desal. Water Treat.*, 248 (2022) 28–38.
- [14] S. Abd El Wanees, A.A. Keshk, Investigation of anodic behavior of nickel in  $H_2SO_4$  solutions using galvanostatic polarization technique. IV. Initiation and inhibition of pitting corrosion by Cl<sup>-</sup> ions and ethoxylated surfactants, *Int. J. Electrochem. Sci.*, 16 (2021) 21087, doi: 10.20964/2021.08.38.
- [15] M. Ball, M. Wietschel, The future of hydrogen-opportunities and challenges, *Int. J. Hydrogen Energy*, 34 (2009) 615–627.
- [16] U.B. Demirci, O. Akdim, P. Miele, Ten-year efforts and a no-go recommendation for sodium borohydride for on-board automotive hydrogen storage, *Int. J. Hydrogen Energy*, 34 (2009) 2638–2645.
- [17] A. Boddien, B. Loges, H. Junge, M. Beller, Hydrogen generation at ambient conditions: application in fuel cells, *Chem. Sus. Chem.*, 1 (2008) 751–758.
- [18] G. Principi, F. Agreste, A. Magdalena, S.L. Russo, The problem of solid-state hydrogen storage, *Int. J. Hydrogen Energy*, 34 (2008) 2087–2097.
- [19] Z.X. Guo, C. Shang, K.F. Aguey-Zinsou, Materials challenges for hydrogen storage, *J. Eur. Ceram. Soc.*, 2828 (2008) 1467–1473.

- [20] M.G.A. Saleh, S. Abd El Wanees, S.K. Mustafa, Dihydropyridine derivatives as controllers for production of hydrogen during zinc dissolution, *Chem. Eng. Commun.*, 206 (2019) 789–803.
- [21] S. Abd El Wanees, A.A.H. Bukhari, N.S. Alatawi, S.K. Khalil, S. Nooh, S.K. Mustafa, S.S. Elyan, Thermodynamic and adsorption studies on the corrosion inhibition of Zn by 2,2'-dithiobis(2,3-dihydro-1,3-benzothiazole) in HCl solutions, *Egypt. J. Chem.*, 64 (2021) 547–559.
- [22] S. Abd El Wanees, A.S. Al-Gorair, H. Hawsawi, M.T. Alotaibi, M.G.A. Saleh, M. Abdallah, S.S. Elyan, Inhibition of pitting corrosion of C-steel in oilfield-produced water using some purine derivatives, *Desal. Water Treat.*, 269 (2022) 21–32.
- [23] S. Abd El Wanees, M.I. Alahmdi, M.A. Alsharif, Y. Atef, Mitigation of hydrogen evolution during zinc corrosion in aqueous acidic media using 5-amino-4-imidazole-carboxamide, *Egypt. J. Chem.*, 62 (2019) 811–825.
- [24] H.Z. Wang, D.Y.C. Leung, M.K.H. Leung, M. Ni, A review on hydrogen production using aluminum and aluminum alloys, *Renewable Sustainable Energy Rev.*, 13 (2009) 845–853.
- [25] S. Abd El Wanees, N.M. El Basiony, A.M. Al-Sabagh, M.A. Alsharif, S.M. Abd El Haleem, M.A. Migahed, Controlling of H<sub>2</sub> gas production during Zn dissolution in HCl solutions, *J. Mol. Liq.*, 248 (2017) 943–952.
- [26] M.A. Deyab, Hydrogen generation during the corrosion of carbon steel in crotonic acid and using some organic surfactants to control hydrogen evolution, *Int. J. Hydrogen Energy*, 38 (2013) 13511–13519.
- [27] S. Abd El Wanees, S. Sada, Corrosion Inhibition of zinc in aqueous acidic media using a novel synthesized Schiff Base-an experimental and theoretical study, *J. Dispersion Sci. Technol.*, 40 (2018) 1813–1826.
- [28] S. Abd El Wanees, M.I. Alahmdi, M. Abd El Azzem, H.E., Ahmed, 4,6-Dimethyl-2-oxo-1,2-dihydropyridine-3-carboxylic acid as an inhibitor towards the corrosion of C-steel in acetic acid, *Int. J. Electrochem. Sci.*, 11 (2016) 3448–3466.
- [29] S. Abd El Wanees, A. Abd El Aal Mohamed, M. Abd El Azeem, R. El Said, Inhibition of silver corrosion in nitric acid by some aliphatic amines, *J. Dispersion Sci. Technol.*, 31 (2010) 1516–1525.
- [30] S. Abd El Wanees, A. Diab, O. Azazy, M.A. El Azim, Inhibition effect of N-(pyridin-2-yl-carbamothioyl) benzamide on the corrosion of C-steel in sulfuric acid solutions, *J. Dispersion Sci. Technol.*, 35 (2014) 1571–1580.
- [31] S. Abd El Wanees, M.I. Alahmdi, S.M. Rashwan, M.M. Kamel, M.G. Abd El Sadek, Inhibitive effect of cetyltriphenylphosphonium bromide on C-steel corrosion in HCl solution, *Int. J. Electrochem. Sci.*, 11 (2016) 9265–9281.
- [32] P. Mourya, P. Singh, R.B. Rastogi, M.M., Singh, Inhibition of mild steel corrosion by 1,4,6-trimethyl-2-oxo-1,2-dihydropyridine-3-carbonitrile and synergistic effect of halide ion in 0.5 M H<sub>2</sub>SO<sub>4</sub>, *Appl. Surf. Sci.*, 380 (2016) 141–150.
- [33] S.M. Abd El Haleem, S. Abd El Wanees, A.B. Radwan, Environmental factors affecting the corrosion behavior of reinforcing steel. V. Role of chloride and sulfate ions in the corrosion of reinforcing steel in saturated Ca(OH)<sub>2</sub> solutions, *Corros. Sci.*, 57 (2013) 1–15.
- [34] A.S. Fouda, A.A. Sh. Al-Sarawy, H.M. Ahmed, F. El-Abbasy, Corrosion inhibition of aluminum 6063 using some pharmaceutical compounds, *Corros. Sci.*, 51 (2009) 485–492.
- [35] A.S. Al-Gorair, S. Abd El Wanees, M.A. Hegazy, S.S. Al-Juaid, K.A. Soliman, M.M. Asab, Experimental and theoretical studies on controlling hydrogen production on C-steel in hydrochloric acid solutions using N<sub>1</sub>,N<sub>1</sub>'-(ethane-1,2-diy) bis(N<sub>2</sub>-(4-(dimethylamino)-benzylidene) ethane-1,2-diamine), *Mater. Chem. Phys.*, 297 (2023) 127351, doi: 10.1016/j.matchemphys.2023.127351.
- [36] S. Abd El Wanees, E.E. Abd El Aal, N-Phenylcinnamimide and some of its derivatives as inhibitors for corrosion of lead in HCl solutions, *Corros. Sci.*, 52 (2010) 338–344.
- [37] A. Jagminas, I. Vrublevsky, J. Kuzmarskyte, V. Jasulaitiene, Composition, structure and electrical properties of alumina barrier layers grown in fluoride-containing oxalic acid solutions, *Acta Mater.*, 56 (2008) 1390–1398.
- [38] M. Abd El Kader, A.M. Shams El Din, Film thickening on nickel in aqueous solutions in relation to anions type and concentration, *Br. Corros. J.*, 14 (1979) 40–44.
- [39] S.M. Abd El Haleem, S. Abd El Wanees, E.E. Abd El Aal, A. Diab, Environmental factors affecting the corrosion behavior of reinforcing steel II. Role of some anions in the initiation and inhibition of pitting corrosion of steel in Ca(OH)<sub>2</sub>, *Corros. Sci.*, 52 (2010) 292–302.
- [40] E.E. Abd El Aal, S. Abd El Wanees, A. Farouk, S.M. Abd El Haleem, Factors affecting the corrosion behavior of aluminum in acid solutions. II. Inorganic additives as corrosion inhibitors for Al in HCl solutions, *Corros. Sci.*, 68 (2013) 14–24.
- [41] S.M. Abd El Haleem, S. Abd El Wanees, A.B. Radwan, Environmental factors affecting the corrosion behavior of reinforcing steel. VI. Benzotriazole and its derivatives as corrosion inhibitors of steel, *Corros. Sci.*, 87 (2014) 321–333.
- [42] S. Abd El Wanees, M.I. Alahmdi, M. Abd El Azzem, H.E. Ahmed, 4,6-Dimethyl-2-oxo-1,2-dihydropyridine-3-carboxylic acid as an inhibitor towards the corrosion of C-steel in acetic acid, *Int. J. Electrochem. Sci.*, 11 (2016) 3448–3466.
- [43] M.A. Ameer, A.M. Fekry, Inhibition effect of newly synthesized heterocyclic organic molecules on corrosion of steel in alkaline medium containing chloride, *Int. J. Hydrogen Energy*, 35 (2010) 11387–11396.
- [44] F.M. Mahgoub, B.A. Abdel-Nabey, Y.A. El-Samadisy, Adopting a multipurpose inhibitor to control corrosion of ferrous alloys in cooling water systems, *Mater. Chem. Phys.*, 120 (2010) 104–108.
- [45] F.M. Al-Kharafi, W.A. Badawy, Corrosion and passivation of Al and Al-Si alloys in nitric acid solutions II—effect of chloride ions, *Electrochim. Acta*, 40 (1995) 1811–1817.
- [46] A. Yurt, S. Ulutas, H. Dal, Electrochemical and theoretical investigation on the corrosion of aluminium in acidic solution containing some Schiff bases, *Appl. Surf. Sci.*, 253 (2006) 919–925.
- [47] Q.B. Zhang, Y.X. Hua, Corrosion inhibition of aluminum in hydrochloric acid solution by alkylimidazolium ionic liquids, *Mater. Chem. Phys.*, 119 (2010) 57–64.
- [48] R.S. Goncalves, D.S. Azambuja, A.M. Serpa Lucho, Electrochemical studies of propargyl alcohol as corrosion inhibitor for nickel, copper, and copper/nickel (55/45) alloy, *Corros. Sci.*, 44 (2002) 467–479.
- [49] K.F. Khaleda, M.M. Al-Qahtani, The inhibitive effect of some tetrazole derivatives towards Al corrosion in acid solution: chemical, electrochemical and theoretical studies, *Mater. Chem. Phys.*, 113 (2009) 150–158.
- [50] E. McCafferty, N. Hackerman, Double layer capacitance of iron and corrosion inhibition with polymethylene diamines, *J. Electrochem. Soc.*, 119 (2002) 146–154.
- [51] A.S. Al-Gorair, S. Abd El Wanees, A.M. Al-bonayan, S.S. Al-Juaid, S. Nooh, M. Abdallah, Investigation of the effect of ClO<sub>4</sub><sup>-</sup> ions on the growth of indium oxide films on in electrode in dilute Na<sub>2</sub>B<sub>4</sub>O<sub>7</sub> solution by potentiometric technique, *Int. J. Electrochem. Sci.*, 17 (2022) 221251, doi: 10.20964/2022.12.51.
- [52] S. Abd El Wanees, A.B. Radwan, M.A. Alsharif, S.M. Abd El Haleem, Initiation, and inhibition of pitting on reinforcing steel under natural corrosion conditions, *Mater. Chem. Phys.*, 190 (2017) 79–95.
- [53] S.M. Abd El Haleem, S. Abd El Wanees, A. Farouk, Hydrogen production on aluminum in alkaline media, *Prot. Met. Phys. Chem. Surf.*, 57 (2021) 906–916.
- [54] S.A. Umoren, M.M. Solomon, U.M. Eduok, I.B. Obot, A.U. Israel, Inhibition of mild steel corrosion in H<sub>2</sub>SO<sub>4</sub> solution by coconut coir dust extract obtained from different solvent systems and synergistic effect of iodide ions: ethanol and acetone extracts, *J. Environ. Chem. Eng.*, 2 (2014) 1048–1060.
- [55] X.-H. Li, S.-D. Deng, H. Fu, G.-N. Mu, Inhibition effect of 6-benzyl amino purine on the corrosion of cold rolled steel in H<sub>2</sub>SO<sub>4</sub> solution, *Corros. Sci.*, 51 (2009) 620–634.
- [56] X.-H. Li, S.-D. Deng, H. Fu, G.-N. Mu, Inhibition by Tween-85 of the corrosion of cold rolled steel in 1.0 M hydrochloric acid solution, *J. Appl. Electrochem.*, 39 (2009) 1125–1135.

- [57] M.A. Hegazy, H.M. Ahmed, A.S. El-Tabei, Investigation of the inhibitive effect of p-substituted 4-(N,N,N-dimethyldodecylammonium bromide)benzylidene-benzene-2-yl-amine on corrosion of carbon steel pipelines in acidic medium, *Corros. Sci.*, 53 (2011) 671–678.
- [58] M.A. Hegazy, Novel cationic surfactant based on triazole as a corrosion inhibitor for carbon steel in phosphoric acid produced by dihydrate wet process, *J. Mol. Liq.*, 2089 (2015) 227–236.
- [59] N.U. Inbaraj, G.V. Prabhu, Corrosion inhibition properties of paracetamol based benzoxazine on HCS and Al surfaces in 1 M HCl, *Prog. Org. Coat.*, 115 (2018) 27–40.